Fingerprinting ash deposits of small scale eruptions by their physical and textural features

R. Cioni [1,2] , C. D'Oriano [1], A. Bertagnini [2]

[1] Dip.to Scienze della Terra, Via Trentino 51, I-09127 Cagliari, Italy

[2] Ist. Nazionale di Geofisica e Vulcanologia, sez. di Pisa, Via Della Faggiola, 32 I-56126, Pisa, Italy

Abstract

Correlation of distal ash deposits with their proximal counterparts mainly relies on chemical and mineralogical characterization of bulk rock and matrix glasses. However, the study of juvenile fragments often reveals the heterogeneity in terms of clast shape, external surface, groundmass texture and composition. This is particularly evident in small-scale eruptions, characterized by a strong variability in texture and relative abundance of juvenile fragments. This heterogeneity introduces an inherent uncertainty, that makes the compositional data alone inadequate to unequivocally characterize the tephra bed. Pyroclast characteristics, if described and quantified, can represent an additional clue for the correct identification of the tephra.

The paper presents morphological, textural and compositional data on the products of an ash eruption from Middle Age activity of Vesuvius, to demonstrate the information that can be extracted from the proposed type of analysis.

Juvenile fragments from five ash layers throughout the studied products were randomly hand-picked, and fully characterized in terms of external morphology, particle outline parameterization, groundmass texture and glass composition. Statistical analysis of shape parameters characterized groups of fragments that can be compared with the other textural and physical parameters. The main result is that the data do not show important cross-correlations, so suggesting that all of these parameters, together with accurate field data are needed for the complete fingerprinting of a tephra bed. We suggest that this approach is especially important for characterizing the products of small scale, compositionally undistinguishable, eruptions and represents the necessary step to deal with before going into more detailed compositional analyses.

Key words: tephrostratigraphic methods; shape parameters; groundmass texture;
mid-intensity eruptions; ash deposits

1. Introduction

Ash deposits produced by explosive volcanic eruptions can be found thousands of kilometers from their source, and represent an important tool for understanding the frequency and the impact of volcanic activity on the environment. Ash deposits are also excellent chronological and stratigraphic markers and have been extensively used to reconstruct the volcanic history of a single volcano or, at a regional scale, to constrain complex stratigraphic sequences within a reliable chronological framework (Narcisi, 1995; Machida, 1999; Shane, 2000). Correlation of distal ash deposits with their proximal counterparts is sometimes problematic because of the lack of exhaustive data on the characteristic features of the their juvenile and lithic components. Chemical and mineralogical characterization of bulk rock and matrix glasses are presently the most used methods in tephra studies. The compositional data are commonly associated with a lithological description of the different components of the tephra bed (xenolithic material, loose juvenile crystals) and of the grain size (Orsi et al., 1992; Donoghue and Neall, 1996; Narcisi, 1996; De Rosa, 1999: Shane et al., 2002; Turney et al., 2004; Wulf et al., 2004; Wastergard, 2005).

The products of mid-to low-intensity eruptions (sub-Plinian, violent strombolian, vulcanian, ash-dominated eruptions) can show variability of the juvenile material (Nakada and Motomura, 1999; Hammer et al., 2000; Cioni et al., 2003). This variability is well expressed in the deposits of some eruptions of Vesuvius, where different types of juvenile fragments can occur at different stratigraphic levels within a same eruption (Fig. 1 a, b, c), or can coexist within the same stratigraphic level (Fig. 1).

In tephra beds characterized by juvenile fragments heterogeneous in terms of external morphology, mineral and glass composition, and groundmass texture, (crystal type, size and content, and clast vesicularity), the compositional data routinely used to describe the juvenile components may be inadequate to unequivocally characterize the tephra bed. Similar problems are associated with the description of ash deposits with juvenile and xenolithic fractions with similar composition, or of those products where the presence of a largely crystallized groundmass reduces the possibility of performing reliable glass analyses. In recent years, the quantitative determination of groundmass textures (Rosi et al., 2004; D'Oriano et al., 2005) has been widely used for investigating the eruptive dynamics of an event (Dellino and La Volpe, 1996; Carey et al., 2000; Cashman and Blundy, 2000; Maria and Carey, 2002). However, this approach also proved very effective for identifying the juvenile fragments of an ash deposit (Taddeucci et al., 2004; Wright et al., 2004), so adding another observational character able

to give a more complete description of a tephra bed. Bearing this in mind, we suggest that in order to obtain an unequivocal fingerprint of the juvenile material proper of a tephra bed, textural and morphological characterization of the juvenile clasts should join the compositional analysis. In this paper we present morphological, textural and compositional data on the products of an ash eruption from Middle Age activity of Vesuvius, as an example used to highlight the large mess of information we can extract from the proposed type of analysis. The selected deposit is considered representative of mid-intensity eruptions able to generate and inject large amounts of ash in the atmosphere, resulting in long-range ash dispersal. To illustrate the potential of the method we use data from proximal deposits where the primary variability of the juvenile component is still well represented and not modified by transport and depositional processes. The deposits of several eruptions of this type, largely homogeneous and repetitive in terms of composition, can be present as individual beds or as cryptotephra(here intended as a tephra horizon invisible to the naked eye) in the distal sedimentary records, and a complete characterization can be resolutive for their recognition and correlation. We suggest that this approach is especially important for characterizing the products of small scale, compositionally undistinguishable, eruptions and represents the necessary step to deal with before going into more detailed compositional analyses.

The term tephra bed is here used as synonym of ash fall deposit, even if the collective term “tephra” is used in the volcanological literature to indicate any product deriving from pyroclastic fragmentation of magma (Bates and Jackson, 1987).

2. The AS1a Eruption of Vesuvius

The Italian case is a good training-ground to test the different techniques for the study and correlation of tephra beds. The Quaternary volcanoes of central and southern Italy are characterized by a wide spectrum of magma compositions, ranging from alkali-potassic, to alkali-sodic, to calcalkaline (Peccerillo, 2005). The products of the volcanic activity from the different centers are often interlayered in the stratigraphic successions of continental and marine settings of the Mediterranean region. In particular, for the Campanian area, the present knowledge of the stratigraphic successions of Phlegrean Fields and Somma-Vesuvius is very detailed (Orsi et al., 1996; Di Vito et al., 1999; Santacroce et al., 2003; Cioni et al., 2007), and the products of many past eruptions are now very well characterized on a compositional and petrographical basis (Pappalardo et al., 1999; Di Vito et al., 2007; Santacroce et al., 2007). The products of the largest eruptions can be easily detected in the distal

sedimentary successions, as they have a compositional fingerprint well described by numerous authors (see Santacroce et al., 2007, for an exhaustive review). These large-scale eruptions, however, are often separated by time intervals of several thousands or hundreds of years, during which the volcanic activity is characterized by low intensity eruptions. In order to obtain a more detailed scanning of the temporal sequence, we need to study also the minor tephra beds or the cryptotephra often present in the distal "archives" (Narcisi, 1996; Calanchi et al., 1998; Siani et al., 2004; Wulf et al., 2004). These products are generally related to eruptions of lower intensity than those responsible for the major tephra beds. These low to mid intensity eruptions have been very frequent at Vesuvius during the last 3500 years (Andronico and Cioni, 2002; Cioni et al., 2007); the related products do not have the peculiar, in some cases unique, magma compositions of the large eruptions (Andronico and Cioni, 2002; Cioni et al. 2007) and present heterogeneous juvenile fractions. For this reason, these deposits can represent an interesting test case in order to verify the application of quantitative textural and morphological studies to the tephra characterization. Several ash deposits related to long-lasting ash emission activity are present in the Middle Age products of Vesuvius (Andronico et al., 1995; Cioni et al., 2007). In particular we focus here on the deposits of an event, named AS1a according to Cioni et al. (2007), occurred shortly after the 512 AD sub plinian eruption. The deposit consists in a succession of five main beds with a total thickness of about 40 cm at a distance of 7 km East from the vent (Fig. 2). In the reference section the deposit overlies an erosive surface at the top of the 512 AD eruption and is represented by fine and coarse ash layers with minor fine lapilli beds. Five samples were collected at different stratigraphic heights (Fig. 2). The deposit is dispersed in the eastern sector of the volcano and it is clearly identifiable up to a distance of 10-12 km from the vent. Cryptotephra of similar age are present in a core drilled inside the Monticchio Lake, Mt Vulture, 100 km East of Vesuvius (Wulf, 2000).

3. Methods

The methods commonly used in volcanology to describe pyroclastic fragments have been widely discussed in many papers since the pioneering studies of Walker and Croasdale (1971) and Heiken (1974). Recently Turney et al. (2004) reconsidered the methods for describing pyroclastic fragments for the drawing up of a general protocol to apply in tephrochronological studies. In this paper, the description and characterization of the fragments of the selected eruption was obtained using a selection and in some cases an improvement of the currently universally used methods, trying to put

together classical methods derived from tephrochronology with some of the recently developed techniques of textural characterization of the fragments.

3.1. Sample preparation

The studied samples were prepared in order to collect a complete set of morphological, textural, and compositional data on each single ash fragment. About 30 juvenile fragments (from the 0.5-1 mm size interval) were randomly hand-picked under the stereomicroscope from each sample. The choice of this grain-size represents a compromise between sample representativeness and suitability of performing reliable analytical work on the single grains. For their identification, the selected clasts were mounted on double-adhesive tape on a glass slide. External morphology of the clasts was then described and the clasts photographed both using a digital camera at the stereomicroscope and at the Scanning Electron Microscope (SEM). The glass slide was then embedded in epoxy resin and polished until a surface approximately containing the maximum diameter of the fragments was exposed. These mounts were used for SEM inspection, back-scattered electrons (BSE) imaging of the textural features and for analytical purposes of the individual clasts.

3.2. Composition

Major elements in minerals and glass were determined by energy dispersive X-ray analysis using EDAX DX4 on a Philips XL30 SEM at the Dipartimento di Scienze della Terra of Pisa, at an accelerating voltage of 20 kV, beam current of 0.1 nA and working distance of 10 mm. In order to reduce Na losses, matrix glass was analyzed in raster mode, using windows in the range from 5x5 μm, in highly crystalline samples, to 10x10 μm. The analytical error measured on mineral and glass standards is always lower than 5-10 wt%, increasing at low concentrations. In order to check for microscopic inhomegeneities of the matrix glass, 2 to 3 raster windows were analyzed in 5 to 10 clasts for each sample, and the results on each clast averaged. Care was used in avoiding areas close less than a few microns to groundmass crystals.

3.3. Clast morphology

Classical observations of clast morphology at the SEM comprised description of particle shape, vesicularity, external surface texture, and eventual occurrence of surface alteration or secondary minerals (Heiken and Wohletz, 1985; Heiken and Wohletz, 1991). Quantitative parameters of ash grain morphology were obtained by processing SEM low magnification images (80x to 100x) on each grain. Four non-dimensional shape parameters were measured on each clast: rectangularity, compactness, elongation and circularity (Fig. 3; Dellino and La Volpe, 1996; Riley et al., 2003). The projection of the particle outline on the horizontal plane was used as a proxy for the particle shape. This outline was then filled and converted into a binary image, and the morphological parameters of interest were measured using the ImageJ software (http://rsb.info.nih.gov/ij)(Fig.3).

3.4. Statistical analysis

The shape parameters were statistically processed using the method of Principal Component Analysis (PCA; Davis, 2003), in order to create classes with similar features. The goal of PCA is to reduce the number of variables into a set of orthogonal maximum linear combinations of the same variables (the new principal components), in order to highlight their similarities and differences. Cluster analysis was then applied to the extracted Principal Components in order to create groups of objects, or clusters, with similar features. By hierarchical clustering it is possible to create cluster trees, in which normalized Euclidean distance (root mean-square distance) is used as a measure of similarity between particles. Results are shown in a dendrogram, that consists of many U-shaped lines connecting objects, where the height of each U depends inversely on the degree of similarity between two connected objects.

3.5. Textural investigations

Two backscattered (BSE) images were captured for each clast at magnification of 250x and resolution of 2048x1600 pixel. Quantitative measures of the groundmass features include vesicle shape, total vesicularity, and crystal content. Vesicle shape and content were obtained by manual reconstruction of the bubble contour, and incipient bubble coalescence was graphically deconvoluted. The circularity and the elongation of the vesicles (defined as in Fig. 3) were calculated using ImageJ software. For automated analysis of groundmass vesicularity, binary images were used to estimate the percent area of vesicles. The same procedure was applied for the quantification of the groundmass crystal content.

Data were recalculated on a vesicle free basis. This automated method possibly shifts toward highest values the upper range of groundmass crystal content, due to the occasional presence in some of the analyzed clasts of phenocrysts which contribute to increase the area occupied by the crystals.

4. Results

In the studied products, the juvenile ash fragments show a large variability in terms of external morphology; vesicle content, size, and shape; and groundmass texture and composition. Macroscopically, ash fragments appear to vary between two end members: from light-brown, highly to moderately vesicular, crystal-poor pumice, to black, poorly vesicular, crystal-rich scoria. In some fragments black scoria is included in light-colored pumice. The different types of juvenile fragments are present in the deposits with proportions which vary with the stratigraphic height. All the data obtained for each studied fragment are reported in Table 1; representative glass composition of the studied fragments is reported in Table 2.

4.1. External morphology

The shapes of juvenile clasts are shown in Fig. 4, mainly based on classical descriptive morphological features of the juvenile fragments (Heiken and Wohletz, 1985). At least three different types of clasts are recognized:

-Spongy clasts. They consist of vesicular fragments with nearly spherical bubbles of similar size intersecting the external surfaces of the clast (Fig.4 a). Clasts vary from highly vesicular with large coalescent bubbles and thin walls to moderately vesicular with less marked coalescence and thicker walls.

-Fused clasts. The fragments are irregularly shaped and show smooth glassy surfaces (Fig.4 b). Vesicles vary from sub-spherical to elongated, they are heterogeneously distributed within the clast and generally not exposed on the external surface. A particular type is represented by drop like clasts with fused surfaces and fluidal forms (“achneliths” according to Walker and Croasdale, 1971; or “droplets” according to Heiken, 1971).

-Blocky clasts. Their overall shape is determined by planar or curviplanar, glassy to microcrystalline surfaces (Heiken and Wohletz, 1985) intersecting few vesicles (Fig.4 c). They have a nearly isometric form (equant to sub-equant grains). Vesicle shape is largely variable, from irregularly shaped to sub-

spherical. Clasts vary from moderately to poorly vesicular. These three types of fragments are present in all the analyzed samples, with variable proportions.

Blocky clasts are the most abundant fragments; they represent the 62 vol % of the sample 3, while in the other samples their abundance vary from 30 to 45 vol %. Spongy clasts are generally restricted to 10 vol % of the total, except in the sample 1 where they reach the 40vol %. The larger variability is shown by fused clasts, that represent the majority (52 vol %) of sample 4.

4.2. Particle outline

Particle outline of each clast is described by the shape parameters listed in Table 1. The cluster analysis was performed using the first two principal components obtained by the multivariate analysis on the different parameter of each clast. These two principal components account for the 97.2% of the total variance. Cluster analysis of the measured shape parameters helps in individuating at least three groups of clasts which include all the particles. Figure 5 shows the external shapes representative of the three recognized groups and the percentage of each group in the different samples. These three groups can be described in terms of the classical grain shape parameters used in sedimentary petrology. According to this terminology, each group can be identified in terms of sphericity and roundness of the clasts (Blatt et al., 1980).

The first group consists of equidimensional (High Sphericity) clasts with uneven outline (Very Angular) (HS-VA). This is the most abundant type, forming the 53 vol % of the analyzed fragments. It always represents the majority of the juvenile fragments also in the single samples, ranging between 40 and 60 vol % in all the analyzed samples.

The second group (HS-SR) contains equidimensional (High Sphericity) particles with smooth outline (Sub-Rounded), and represents the 16 vol % of the total. It reaches the maximum value (30 vol %) in sample 1, decreasing until the 9 vol % at the top of the succession.

Particles of the third group (LS-VA) are elongated (Low Sphericity)fragments with uneven outline (Very Angular), and represent the 31 vol % of the total fragments, showing a quite constant abundance (26-38 vol %) along the succession.

4.3. Compositional features

The juvenile component has a phonolitic tephrite bulk composition. Groundmass glass is a foidite, with a lower SiO2 content and a larger range of alkali than bulk rock. Juvenile material is porphyritic with leucite, clinopyroxene and phlogopite, while the groundmass consists of microphenocrysts and microlites of leucite, and microlites of pyroxene and plagioclase. These compositional features are very common in the products of violent strombolian and ash emission activity of Vesuvius(Santacroce et al., 1993; Marianelli et al., 1999; Andronico and Cioni, 2002; Santacroce et al., 2007). The concentration of the oxides of the major elements in groundmass glass is fully comparable with the compositional range shown by the 472 AD (Santacroce et al., 2007), and partially overlaps the composition of 512 AD (Fig.6), being not completely distinguishable from them on a pure compositional basis(Table 2).

4.4. Groundmass texture

Groundmass textures are described in terms of vesicle and crystal content, and vesicle size. Three different groups of fragments are generally recognized in all the samples, having different relative abundances.

-Moderately Vesicular, Glassy clasts (MVG). Clasts are characterized by a vesicularity index (Houghton and Wilson, 1989) ranging between 35 and 50 vol %. Vesicle mean diameter ranges between 40 and 90 μm at the base of the stratigraphic succession, regularly decreasing toward the top (between 20 and 45 μm). Bubbles are irregularly shaped; in some clasts flattening of bubbles results in a pseudofluidal structure. Cumulative size population density of all the measured vesicles has a bell-shaped distribution skewed toward the largest values(Fig. 7 a). Small, rounded vesicles are also present, recorded by the fine tail of the vesicle distribution. The crystal content is largely variable, ranging between 33 and 80 vol %, with the most frequent values around 55-75 vol %. MVG clasts are the most abundant type of fragments, representing the 44 vol % of the whole dataset, ranging between 30 vol % in the layer L2 (Fig. 2) to 70 vol % in the layer L4. Glass composition is homogeneous both at the scale of a single fragment and between the different fragments of this type (Fig. 7 a).

-Poorly Vesicular, Glassy clasts (PVG). They are characterized by a vesicularity index ranging between 15-30 vol % (Fig.7 b). The mean diameter of the vesicles ranges between 35 and 75 μm at the base of the succession, decreasing to 20-35 μm at the top. Bubbles are nearly spherical, and do not evidence coalescence. In some fragments collapsed bubbles are present. The generally smaller dimension of bubbles with respect to MVG clasts results in a size population density distribution more symmetrical and peaked at a smaller size (Fig. 7 b). Crystal content has a similar range than MVG (55-85 vol %).

This is possibly related to the similar crystal content of the two types of fragments. PVG clasts represent the 35 vol % of the total fragments; they are the most abundant type of fragments at the base of the succession (L1, Fig. 2), regularly decreasing from 54 vol % to 20 vol % at top of the succession (L4, Fig. 2). Glass composition is homogeneous, being very similar to that of the MVG clasts.

-Dense, Crystal-Rich clasts (DCR). They are characterized by a crystal content > 90 vol % and vesicularity lower than 30 vol % (Fig.7 c). The vesicle diameter ranges between 20 and 65 μm, increasing toward the top of the succession. Bubbles are irregularly shaped, reflecting crystal growth on the bubble walls. Round vesicles smaller than 5 μm diameter are present in nearly holocrystalline fragments, suggesting a final vesiculation possibly induced by extreme crystal nucleation and growth. Population density of bubbles lacks the very pronounced modes of MVG and PVG clasts, showing a platykurtic distribution and a dimensional range of the vesicles similar to the other two clast types. DCR clasts are the less abundant type of fragments (20 vol % of the total). They are the most abundant type in layer L2 (42 vol%), while poorly represented in the other layers (from 3 to 10 vol%). Glass composition is largely variable between the different samples, and some oxides show different concentrations with respect to MVG and PVG clasts (Fig. 7c).

4.5. Relationships between the different parameters

The discussed morphological and textural features represent a dataset which exhaustively describes the juvenile fraction of each studied sample. While the relative abundance of the different classes described above for each observed feature (external morphology, particle outline, groundmass composition and texture) is dependent on the grain size selected for the study, these classes well represent the variability of the juvenile material from few millimeters to a hundred microns (fine lapilli to fine ash, according to the grain size terminology introduced by White and Houghton, 2006). Cross-correlation between the different measured parameters is shown in Fig. 8 for two of the studied samples. Within a same sample, we observe no clear mutual relationships between the different parameters. The main result is that a one-to-one correlation between the parameters does not exist so that, while for example all the DCR clasts of sample EP2 have blocky morphology (Fig.8 g), the blocky clasts of the same sample are characterized by variable groundmass texture (Fig. 8 a). Apparently, the commonly used classification based on external morphology of the clasts (Heiken, 1974) is not suited to differentiate clasts with similar characteristics of the groundmass texture (Fig. 8 a, b). In the presented study, for example, while spongy and fused clasts of sample EP2 mainly belong to MVG category, the same fragments of

sample EP4 practically cover the whole spectrum of groundmass textures (Fig. 8 a, b). Surprisingly, the classes of particle outline do not show a correlation with the morphological features of the external surface of the clast (Fig. 8e, f). Similarly, particle outline of the clasts is completely uncorrelated with groundmass texture (Fig. 8 c, d). This suggests that the classes of particle outline as derived from the proposed method of cluster analysis represent an additional good descriptor for juvenile particles of the tephra, being completely independent from all the other measured parameters. A clear correlation exists between the three categories of groundmass texture and composition of the residual glass, as clearly shown in Figure 7. This correlation should be taken in account when trying to describe the whole compositional spectrum typical of a given tephra bed. A quick, low cost estimation of the relative proportions of the different compositional classes of clasts could be done by observation of thin section or back scattered electron images of a set of randomly chosen juvenile fragments.

5. Concluding Remarks

The methods generally adopted for tephrostratigraphic correlations mainly rely on the comparison (sometimes poorly representative on a statistical basis) of the composition of a distal tephra bed with the existing dataset of selected possible sources. The comparison is often made between data collected with different analytical methods, making the correlation sometimes very problematic. In addition, the compositional data on glassy fragments commonly available in the volcanological literature are rarely associated to descriptive data on textural and morphological features of the fragments. This can reveal an important pitfall when using the data for correlation purposes, especially because the detailed study of randomly selected juvenile fragments also from single beds of a pyroclastic deposit often testify to a very large variability in terms of clast shape, external surface, groundmass texture and composition. While this variability is generally present in all types of eruptions, the relative abundance of the different categories of clasts within a single bed widely varies. Large-scale, Plinian-type eruptions are generally dominated by only few, poorly variable, pumice types. Conversely, small-scale, sub-plinian to violent strombolian to ash-dominated eruptions often lack a largely predominant type of juvenile material in terms of physical and compositional features, and all the different types of fragments are unevenly distributed along the succession of the deposits. In addition,the relative proportions of the different types of juvenile material can be strongly affected by transport and deposition (eolian fractionation; Fisher and Schmincke, 1984). Despite this, textural and compositional variability of the juvenile material can be still preserved, even if in proportions variable with distance, in the distal

counterparts of such deposits. The presence of different types of juvenile fragments in a tephra bed introduces an inherent uncertainty when correlations are only based on glass composition of not clearly identified juvenile fragments. Conversely, this variability represents an additional feature to be used for a more in-depth characterization of the tephra bed and, if opportunely described and quantified, can represent a decisive clue for the correct identification and correlation of the tephra bed. The proposed methodology of physical and compositional fingerprinting of ash deposits includes a set of parameters that can be used as a collective, unequivocal descriptor of the juvenile material. An important result of the analysis on the AS1a deposit is that the measured parameters (external morphology, particle outline, groundmass texture, glass composition) do not show remarkable cross-correlations, so being all useful to a complete description of juvenile material. This also suggests that provenance studies on heterogeneous ash deposits need a combination of analytical and field data to constrain the origin of the products.

A conclusive message to be delivered to the volcanological community is that, when studying the deposits of an explosive eruption, volcanologists should bear in mind that their data will be possibly used in tephrostratigraphic studies as the main source for tracing correlations between proximal and distal tephra beds. From this point of view the proposed methodology, as it provides a more accurate picture of the whole spectrum of fragments, reveals very useful not only for deriving information about the dynamics of magma ascent, fragmentation, transport and deposition, but also for tephrostratigraphic purposes.

Acknowledgements

This work has been developed in the frame of the INGV-DPC project V3_4 Vesuvio, Fundings to R. Cioni. We thank R. De Rosa, G. Heiken and R. Sulpizio for their careful reviews and constructive suggestions.

References

Andronico D, Calderoni G, Cioni R, Sbrana A, Sulpizio R, Santacroce R (1995) Geological map of Somma-Vesuvius volcano. Per Mineral 64:77–78

Andronico, D., Cioni, R., 2002. Contrasting styles of Mount Vesuvius activity in the period between the Avellino and Pompeii Plinian eruptions, and some implications for assessment of future hazards. Bulletin of Volcanology 64, 372– 391.

Bates, R.L., and Jackson, J.A., 1987. Glossary of geology (3rd ed.). Alexandria Edition, Va., American Geological Institute, 788 p.

Blatt, H., Middleton, G., Murray, R., 1980. Origin of sedimentary rocks. Prentice-Hall, NJ. 782 p.

Calanchi, N., Cattaneo, A., Dinelli, E., Gasparotto, G., Lucchini, F., 1998. Tephra layers in Late Quaternary sediments of the central Adriatic Sea. Marine Geology 149, 191-209.

Carey, S., Maria, A., Sigurdsson, H., 2000. Use of fractal analysis for discrimination of particles from primary and reworked jökulhlaup deposits in SE Iceland. Journal of Volcanology and Geothermal Research 104, 65-80.

Cashman, K.V., Blundy J., 2000. Degassing and crystallization of ascending andesite and dacite. Philosophical Transactions of the Royal Society of London 358, 1487–1513.

Cioni R., Sulpizio, R., Garruccio, N., 2003. Variability of the eruption dynamics during a Subplinian event: the Greenish Pumice eruption of Somma-Vesuvius (Italy). J. Volcanol. Geotherm. Res. 124, 89-114.

Cioni, R., Bertagnini, A., Santacroce, R., Andronico, D., 2007. Explosive activity and eruption scenarios at Somma-Vesuvius (Italy): a review. Journal of Volcanology and Geothermal Research, this issue.

D'Oriano, C., Poggianti, E., Bertagnini, A., Cioni, R., Landi, P., Polacci, M., Rosi, M., 2005. Changes in eruptive style during the A.D. 1538 Monte Nuovo eruption (Phlegrean Fields, Italy): the role of syn-eruptive crystallization. Bulletin of Volcanology 67, 601-621.

Davis, J.C., 2003. Statistics and data analysis in geology, John Wiley and Sons, 638 p.

De Rosa R. (1999) compositional modes in the ash fraction of some modern pyroclastic deposits: their determination and significance. Bull. Volcanol., 61 DOI10.1007/s004450050269, 162-173

Dellino, P., La Volpe, L., 1996. Image processing analysis in reconstructing fragmentation and transportation mechanism of pyroclastic deposits. The case of Monte Pilato – Rocche Rosse eruptions, Lipari (Aeolian islands, Italy). Journal of Volcanology and Geothermal Research 71, 13-29.

Di Vito, M.A., Sulpizio, R., Zanchetta, G., D'Orazio, M., 2007. The late Pleistocene pyroclastic deposits of the Campanian Plain: new insights into the
explosive activity of Neapolitan volcanoes. J. Volcanol. Geotherm. Res., this issue.

Di Vito M.A., Isaia R., Orsi G., Southon J., de Vita S., D'Antonio, M., Pappalardo L., Piochi M., 1999. Volcanism and deformation since 12,000 years at the Campi Flegrei caldera (Italy). J. Volcanol. Geotherm. Res., Special Issue "Volcanism in the Campi Flegrei" Orsi G., Civetta L., Valentine G.A. (Eds)., 91 (2-4): 221-246.

Donoghue, S.L., Neall, V.E., 1996. Tephrostratigraphic studies at Tongariro volcanic centre, New Zealand: an overview. Quaternary International 34-36, 13-20.

Hammer, J.E., Cashman, K.V., Voight, B., 2000. Magmatic processes revealed by textural and compositional trends in Merapi dome lavas. Journal of Volcanology and Geothermal Research 100, 165-192.

Heiken, G. and Wohletz, K., 1991. Fragmentation processes in explosive volcanic eruptions. In *Sedimentation in Volcanic Settings* (R. V. Fisher and G. Smith, eds.), Soc. Econ. Paleont. and Mineral. Spec. Pub.45: 19-26.

Heiken, G., 1974. An atlas of volcanic ash. Smithsonian Contributions of Earth Science 12, 1–101.

Heiken, G., Wohletz, K.H., 1985. Volcanic Ash. University of California Press, Berkeley, California, 245p.
Houghton BF, Wilson CJN (1989) A vesicularity index for pyroclastic deposits. Bull Volcanol 51:451–462

Machida, H., 1999. The stratigraphy, chronology and distribution of distal marker-tephras in and around Japan. Global and Planetary Change 21, 71-94.

Maria, A., Carey, S., 2002. Using fractal analysis to quantitatively characterize the shape of volcanic particles. Journal of Geophysical Research 107 (B11), 2283, doi:10.1029/2001JB000822.

Marianelli P., Metrich N., Sbrana A. (1999) Shallow and deep reservoirs involved in the magma supply of the 1944 eruption of Vesuvius Bulletin of Volcanology 61 48-63

Nakada, S., Motomura, Y., 1999. Petrology of the 1991-1995 eruption at Unzen: effusion pulsation and groundmass crystallization. Journal of Volcanology and Geothermal Research 89, 173-196.

Narcisi, B., 1996. Tephrochronology of a late quaternary lacustrine record from the Monticchio maar (Vulture volcano, southern Italy). Quaternary Science Review 15, 155-165.

Obenholzner, J. H. and Heiken, G. , 1999. Pyroclast textures in the Triassic Rio Fontanaz Tuff—similarities of vesiculation and fragmentation with the Quaternary Campanian Ignimbrite. Acta Vulcanologica, 11: 283-292.

Orsi, G., De Vita, S., Di Vito, M.A., 1996. The restless, resurgent Campi Flegrei nested caldera (Italy): constraints on its evolution and configuration. Journal of Volcanology and Geothermal Research 74, 179–214.

Orsi, G., Gallo, G., Heiken, G., Wohletz, K., Yu, E., and Bonani, G., 1992. A comprehensive study of pumice formation and dispersal: the Cretaio Tephra of Ischia (Italy). Jour. Volc. and Geotherm. Res., 53: 329-354.

Pappalardo L., Civetta L., D'Antonio M., Deino M., Di Vito M., Orsi G., Carandente A., de Vita S., Isaia R. & Piochi M. (1999). Chemical and Sr isotopical evolution of the Phlegraean magmatic system before the Campanian Ignimbrite and the Neapolitan Yellow Tuff eruptions. J. Volcanol. Geotherm. Res., Special Issue "Volcanism in the Campi Flegrei" Orsi G., Civetta L., Valentine G.A. (Eds), 91 (2-4): 141-166.

Peccerillo, A., 2005. Plio-Quaternary volcanism in Italy. Petrology, geochemistry, geodynamics. Springer, Heidelberg, 365 p.

Riley, C.M., Rose, W.I., Bluth, G.J.S., 2003. Quantitative shape measurements of distal volcanic ash. Journal of Geophysical Research 108 (B10), 2504, doi:10.1029/2001JB000818.

Rosi, M., Landi, P., Polacci, M., Di Muro, A., Zandomeneghi, D., 2004. Role of conduit shear on ascent of the crystal-rich magma feeding the 800-year-b.p. Plinian eruption of Quilotoa Volcano (Ecuador). Bulletin of Volcanology 66, 307-321.

Santacroce, R., Cioni, R., Sulpizio, R., Zanchetta, G., Donahue, D. J., Joron, J. L., Marianelli, P., Sbrana, A., 2007. Age and whole rock-glass compositions of proximal pyroclastics from the major explosive eruptions of Somma-Vesuvius: a review as a tool for distal tephrostratigraphy. J. Volcanol. Geotherm. Res., this issue.

Santacroce, R., Sbrana, A., Andronico, D., Cioni, R., Di Vito, A., Marianelli, P., Sulpizio, R., Zanchetta, G., Arrighi, S., Benvenuti, E., Gurioli, L., Leoni, F. M., Luperini, W., 2003. Carta Geologica del Vesuvio, scala 1:15.000. S.E.L.C.A. Firenze.

Shane, P., 2000. Tephrochronology: a New Zealand case study. Earth-Science Reviews 49, 223–259.

Shane, P., Lian, O.B., Augustinus, P., Chisari, R., Heijnis, H., 2002. Tephrostratigraphy and geochronology of ca. 120 Ka terrestrial record at Lake Poukawa, North Island, New Zealand. Global and Planetary Change 33, 221-242.

Siani, G., Sulpizio, R., Paterne, M., Sbrana, A., 2004. Tephrostratigraphy study for the last 18000 14C years in a deep-sea sediment sequence for the South Adriatic. Quaternary Science reviews 23, 2485-2500.

Taddeucci, J., Pompilio, M., Scarlato, P., 2004. Conduit processes during the July-August 2001 explosive activity of Mt. Etna (Italy): inferences from glass chemistry and crystal size distribution of ash particles. Journal of Volcanology and Geothermal Research 137, 1-3 [SPECIAL ISSUE], 33-54.

Turney, C.S.M., Lowe, J., Davies, S.M., Hall, V., Lowe, D.J., Wastegard, S., Hoek, W.Z., Alloway, B., 2004. Tephrochronology of Last Termination Sequences in Europe: a protocol for improved analytical precision and robust correlation procedures (a joint SCOTAV–INTIMATE proposal). Journal of Quaternary Science 19(2), 111–120.

Walker, G.P.L., Croasdale, R., 1971. Characteristics of some basaltic pyroclastics. Bulletin of Volcanology 35, 303–317.

Wastegard, S., 2005. Late Quaternary tephrochronology of Sweden: a review. Quaternary International 130, 49-62.

White, J.D.L., Houghton, B.F., 2006. Primary volcaniclastic rocks. Geology 34, 677-680.

Wright, H.M., Mothers, P., Hall, M.L., Cashman, K.V., 2004. Ash characterization of 1999-present eruptions of Tungurahua Volcano, Ecuador. IAVCEI General Assembly Pucon, Chile.

Wulf S., 2000. Das tephrochronologische Referenzprofil des Lago Grande di Monticchio. Eine detaillierte Stratigraphie des suditalienischen explosiven Vulkanismus der letzen 100.000 Jahre. Dissertation der Doktorat, 125 p.

Figure captions

Fig.1: Comparison between ash grains from selected eruptions of Vesuvius. For each eruption representative juvenile particles with different textural features are shown. Backscattered (BSE) images: A) ash from the air-fall deposit of the 472 AD Pollena eruption. B) ash from the final surge deposits of the 472 AD Pollena eruption. C) ash from the air-fall deposit of 512 AD eruption); D) ash from the air-fall deposit of AS1a eruption.

Fig.2: Stratigraphic section of the Middle Age AS1a deposits at Terzigno, 7 km East of Vesuvius. The deposit, consisting of 4 main beds (from L1 to L4) lies on the erosive surface at the top of the 512 AD sequence and is covered by the deposit of AS1b. The stratigraphic position of the analysed samples is also indicated (EP8 to EP2).

Fig.3: Secondary electrons SEM image processed and made binary for measuring the external shape parameters (rectangularity, compactness, elongation and circularity). Dimensional features and shape parameters are defined.

Fig.4: Secondary electrons SEM images showing the external morphologies of the ash particles. For each group, the two pictures represent the end-member in terms of vesicle shape and content. a) Spongy clasts ; b) fused clasts; c) blocky clasts.

Fig.5: The three groups of particle outlines as derived from the cluster analysis. Numbers refer to the relative abundance of the different groups in the investigated samples. The name of each group is defined by combining terms describing sphericity and angularity of the particles. 1) High Spherical and Very Angular fragments (HS-VA); 2) High Spherical and Sub-Rounded fragments (HS-SR); 3) Low Spherical and Very Angular fragments (LS-VA).

Fig.6: Box plots of major element contents in groundmass glass of 472 AD, 512 AD and AS1a eruptions. Each box encloses 50% of the data (the median value of the variable is displayed as a line). The lines extending from each box mark the minimum and maximum values of the data set that fall within an accepted range. Outliers are displayed as individual points.

Fig.7: Summary of the measured physical and compositional parameters for a) the moderately vesicular glassy clasts (MVG), b) poorly vesicular glassy clasts (PVG) and c) dense crystal-rich clasts (DCR).

From the top of the figure: external morphology, internal texture, groundmass texture, crystal content vs vesicle content (the box represents the range of variability for the corresponding type); cumulative vesicle size population density; major oxides composition.

Fig.8: Cross-correlations between the different measured parameters for samples EP2 and EP4. a and b) external morphology vs. internal texture; c and d) shape parameters vs. internal texture; e and f) shape parameters vs. external morphology; g and h) internal texture vs. external morphology.

Table 1: Measured parameters (mean and standard deviation) of each analysed particle. Rectangularity, Compactness, Elongation, Circularity, Vesicularity (%), crystal content (%), particle outline, external morphology, groundmass texture.

Table 2: Average groundmass glass composition of the three groups of fragments with different internal texture. The number of analyses for each group (in brackets) and the standard deviation (σ) are reported.

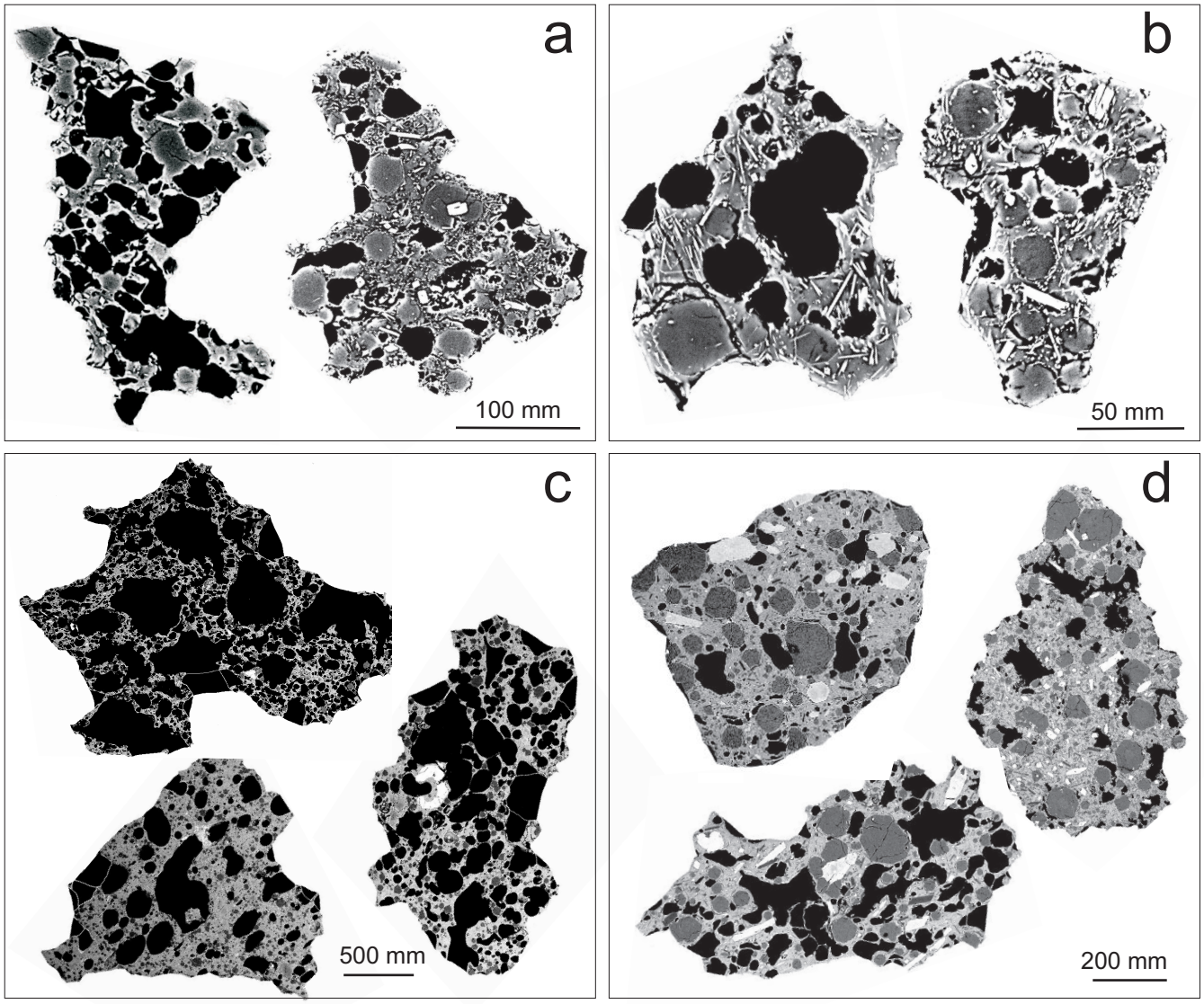
a
100 mm
b
50 mm
c
500 mm
d
200 mm

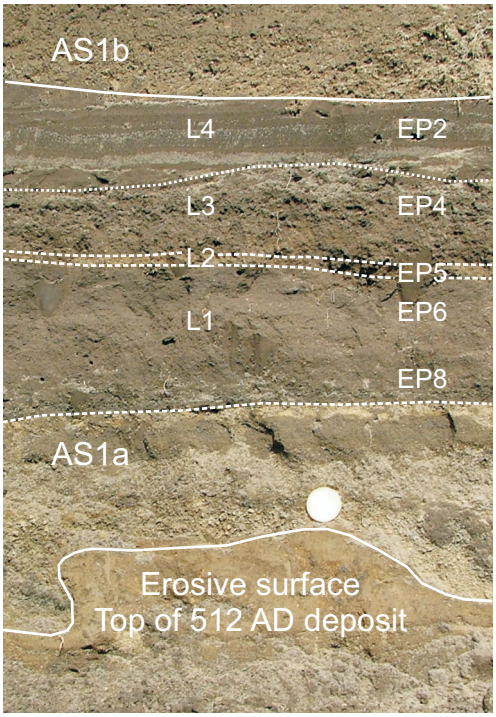
AS1b
L4
EP2
L3
EP4
L2
EP5
EP6
L1
EP8
AS1a
Erosive surface
Top of 512 AD deposit

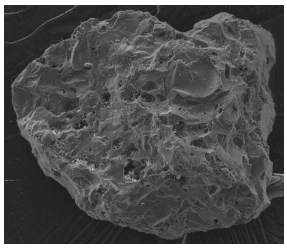

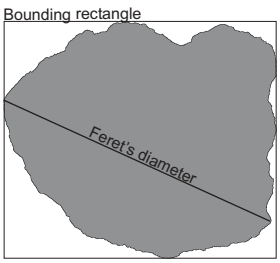

Measured dimensional features:

Area=Area of selection in square pixels. Area is in calibrated units

Perimeter=The length of the outside boundary of the selection

Bounding Rectangle=The smallest rectangle enclosing the selection.

Feret's Diameter=The longest distance between any two points along the selection boundary.

Rectangularity= Particle perimeter/ perimeter of the bounding rectangle

Compactness= particle area/area of the bounding rectangle

Elongation= particle area/Feret's diameter

Circularity= particle perimeter/perimeter of the circle of the same area of the particle

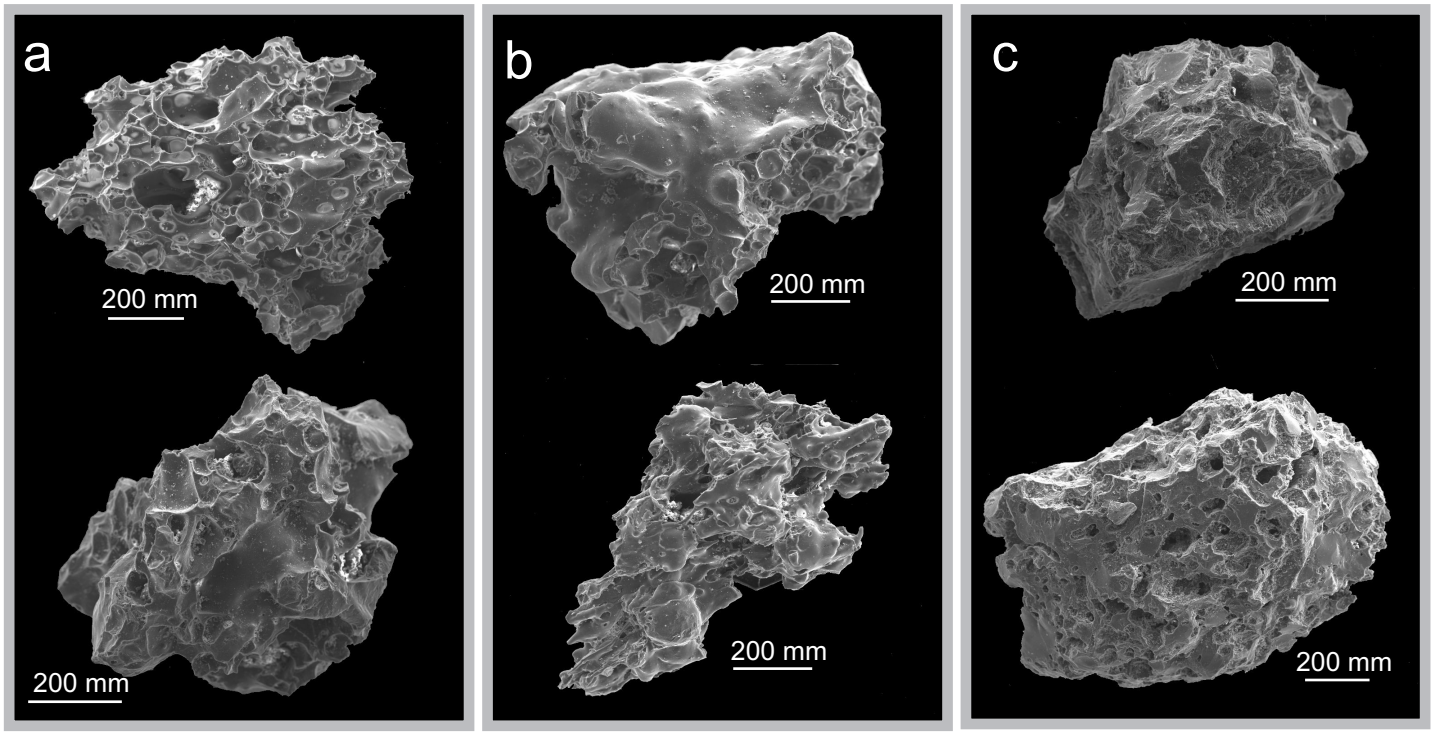
a
200 mm
200 mm
b
200 mm
200 mm
c
200 mm
200 mm

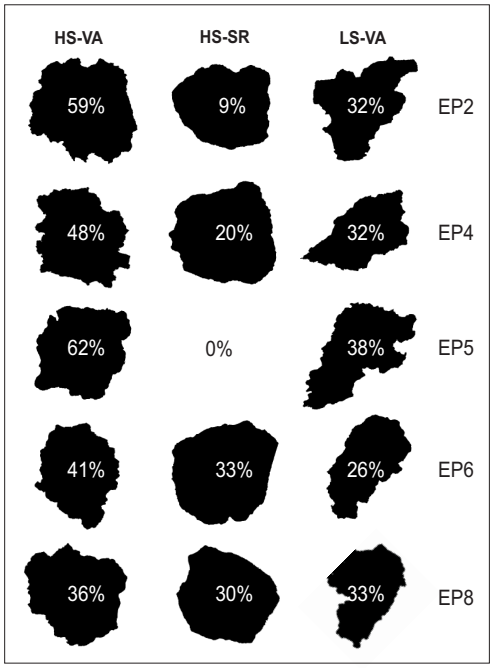
HS-VA
HS-SR
LS-VA
59%
9%
32%
EP2
48%
20%
32%
EP4
62%
0%
38%
EP5
41%
33%
26%
EP6
36%
30%
33%
EP8

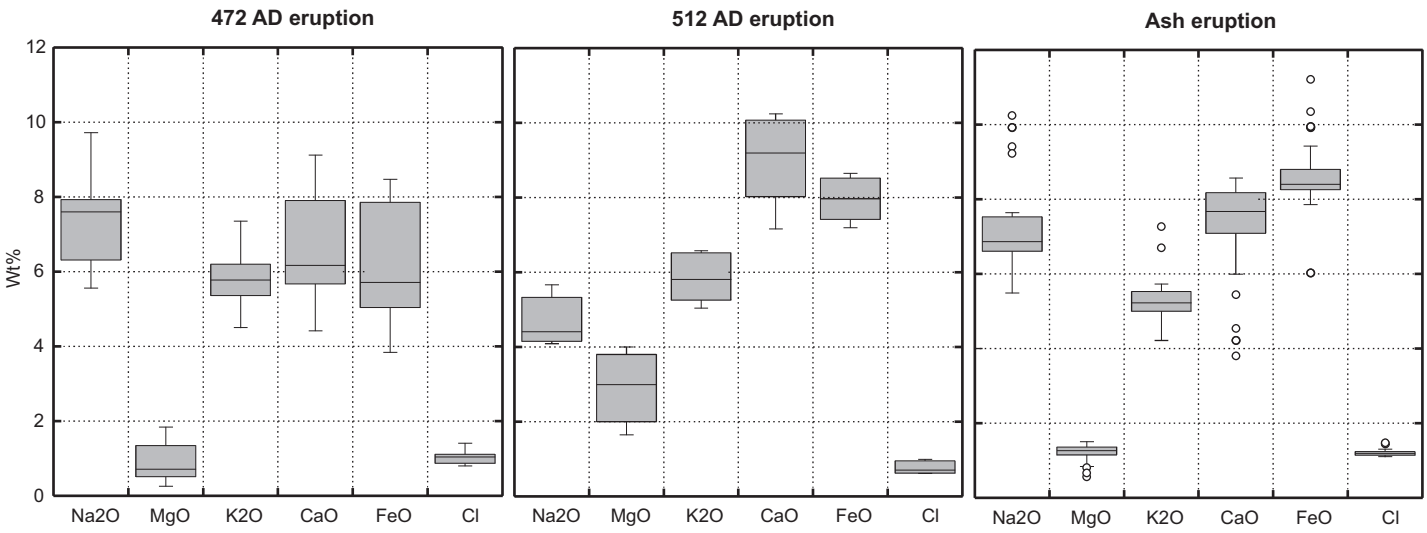
472 AD eruption
512 AD eruption
Ash eruption
Wt%
0
2
4
6
8
10
12
Na2O
MgO
K2O
CaO
FeO
Cl

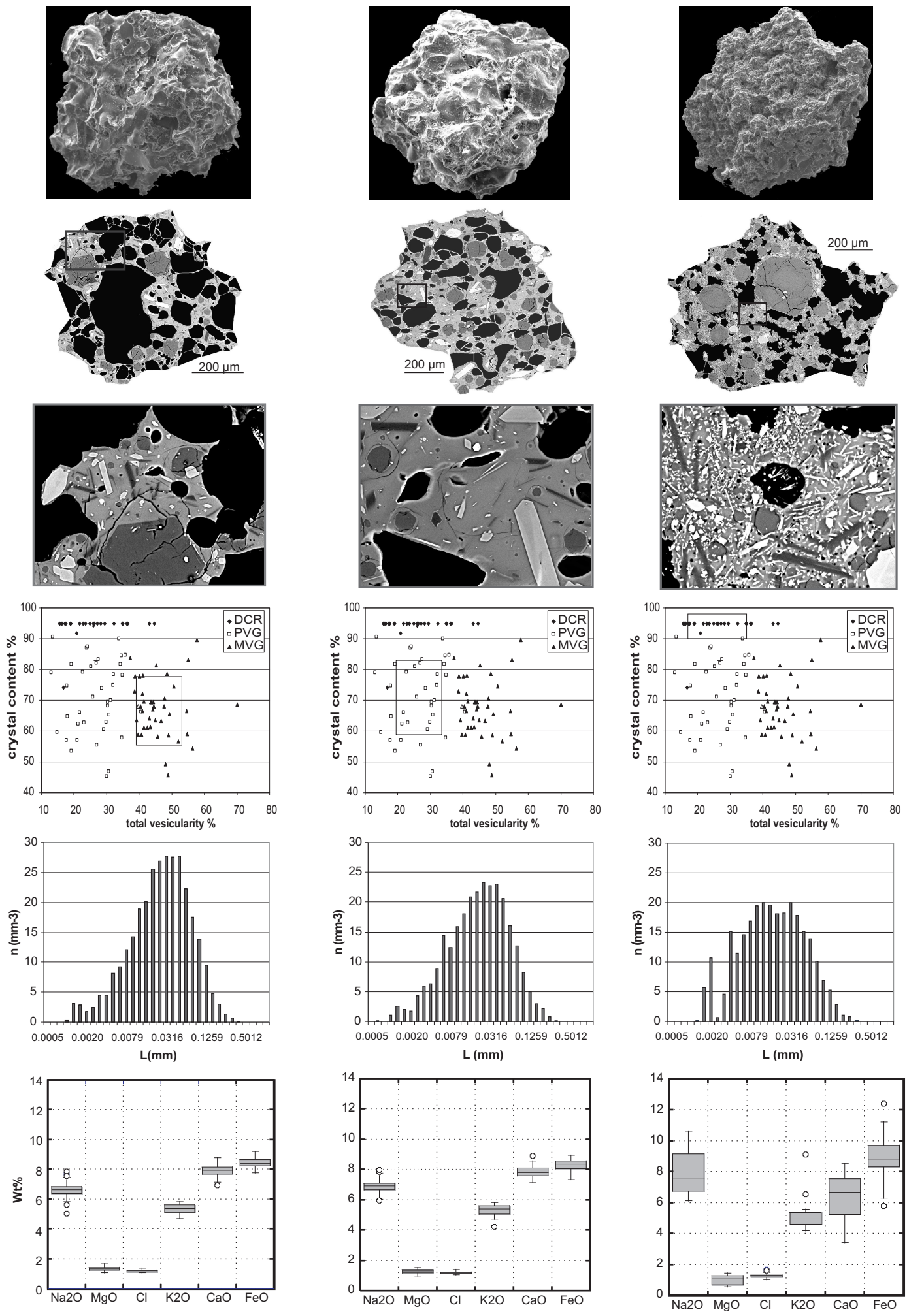
a
b
c
200 µm
200 µm
200 µm
DCR
PVG
MVG
crystal content %
total vesicularity %
n (mm-3)
L(mm)
L (mm)
Wt%
Na2O
MgO
Cl
K2O
CaO
FeO

EP2

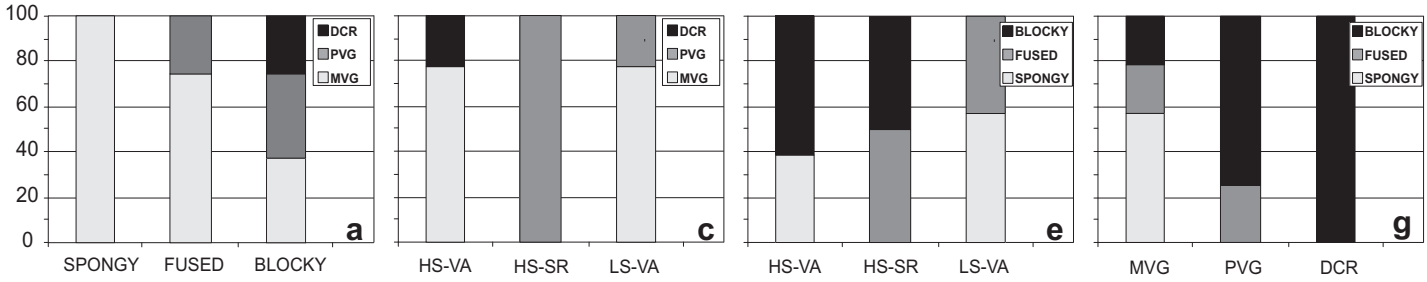
100
80
60
40
20
0
DCR
PVG
MVG
a
SPONGY
FUSED
BLOCKY
c
HS-VA
HS-SR
LS-VA
BLOCKY
FUSED
SPONGY
e
HS-VA
HS-SR
LS-VA
g
MVG
PVG
DCR

EP4

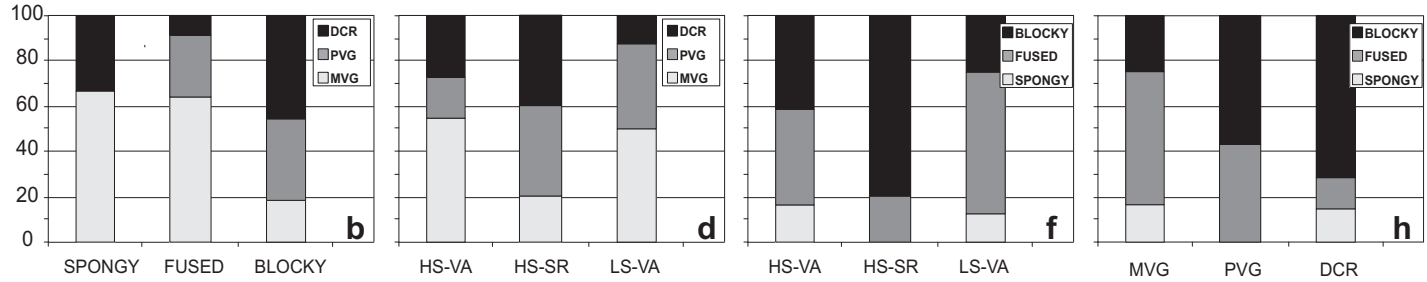
100
80
60
40
20
0
DCR
PVG
MVG
b
SPONGY
FUSED
BLOCKY
d
HS-VA
HS-SR
LS-VA
BLOCKY
FUSED
SPONGY
f
HS-VA
HS-SR
LS-VA
h
MVG
PVG
DCR

SAMPLE	Rect.	Compact.	Elong.	Circ.	%ves.	%xls	Particle outline	ext. morpho.	Ground. Texture
EP2_1	0.938	0.776	1.720	1.205	15	60	HS-SR	blocky	PVG
EP2_2	0.983	0.731	2.059	1.301	40	68	HS-VA	blocky	MVG
EP2_3	0.981	0.766	1.830	1.267	30	69	HS-SR	fused	PVG
EP2_4	0.930	0.688	1.906	1.265	49	46	HS-VA	blocky	MVG
EP2_5	0.956	0.661	1.706	1.329	42	61	HS-VA	spongy	MVG
EP2_6	0.961	0.652	2.061	1.345	36	85	HS-VA	blocky	PVG
EP2_7	1.068	0.613	2.084	1.548	45	81	LS-VA	fused	MVG
EP2_8	1.059	0.727	1.811	1.408	51	74	LS-VA	spongy	MVG
EP2_9	0.995	0.679	2.274	1.368	46	58	HS-VA	spongy	MVG
EP2_10	0.937	0.613	2.402	1.364	n.d.	n.d	HS-VA	blocky	n.d
EP2_11	0.998	0.594	2.185	1.466	n.d.	n.d	HS-VA	spongy	n.d
EP2_12	1.147	0.597	2.171	1.682	39	64	LS-VA	spongy	MVG
EP2_13	0.965	0.610	2.231	1.400	44	69	HS-VA	spongy	MVG
EP2_14	0.977	0.679	1.865	1.345	17	>90	HS-VA	blocky	DCR
EP2_15	0.910	0.656	1.874	1.274	23	>90	HS-VA	blocky	DCR
EP2_17	1.056	0.605	2.333	1.552	48	49	LS-VA	fused	MVG
EP2_18	0.954	0.640	2.137	1.346	18	65	HS-VA	blocky	PVG
EP2_19	1.079	0.525	2.297	1.681	53	33	LS-VA	fused	MVG
EP2_20	0.920	0.655	2.114	1.296	43	61	HS-VA	blocky	MVG
EP2_21	1.023	0.550	2.701	1.559	41	59	LS-VA	spongy	MVG
EP2_23	0.971	0.575	2.064	1.450	41	61	HS-VA	spongy	MVG
EP2_24	1.067	0.721	1.726	1.419	70	69	LS-VA	spongy	MVG

SAMPLE	Rect.	Compact.	Elong.	Circ.	%ves.	%xls	Particle outline	ext. morpho.	Ground. Texture
EP5_1	1.016	0.574	2.531	1.516	31	70	LS-VA	fused	PVG
EP5_2	1.052	0.747	2.016	1.374	36	>90	HS-VA	blocky	DCR
EP5_4	0.894	0.689	1.759	1.216	23	79	HS-VA	blocky	PVG
EP5_5	1.020	0.611	2.139	1.474	n.d	n.d.	LS-VA	fused	n.d
EP5_6	0.889	0.674	1.633	1.223	16	>90	HS-VA	blocky	DCR
EP5_7	1.021	0.557	2.548	1.551	32	78	LS-VA	fused	PVG
EP5_8	1.036	0.594	2.928	1.536	43	64	LS-VA	fused	MVG
EP5_9	0.881	0.701	1.727	1.192	16	>90	HS-VA	blocky	DCR
EP5_10	0.861	0.624	1.796	1.233	n.d.	n.d.	HS-VA	blocky	n.d
EP5_11	0.974	0.657	2.092	1.370	17	74	HS-VA	blocky	PVG
EP5_12	0.956	0.701	1.786	1.290	32	>90	HS-VA	blocky	DCR
EP5_13	0.903	0.643	2.052	1.274	21	92	HS-VA	blocky	PVG
EP5_14	0.938	0.718	1.810	1.255	55	66	HS-VA	blocky	MVG
EP5_15	1.160	0.522	3.260	1.813	44	69	LS-VA	fused	MVG
EP5_16	0.956	0.744	1.623	1.251	17	>90	HS-VA	blocky	PVG
EP5_17	1.008	0.591	2.604	1.480	39	73	LS-VA	fused	MVG
EP5_19	1.122	0.653	1.702	1.567	22	66	LS-VA	blocky	PVG
EP5_20	0.983	0.713	1.673	1.318	13	91	HS-VA	blocky	PVG
EP5_21	0.894	0.662	1.693	1.240	45	>90	HS-VA	blocky	DCR
EP5_22	1.053	0.796	1.772	1.340	16	>90	HS-VA	blocky	DCR
EP5_23	1.041	0.629	2.325	1.486	27	>90	LS-VA	spongy	DCR
EP5_24	1.136	0.732	2.017	1.505	44	67	LS-VA	spongy	MVG
EP5_25	0.949	0.629	2.302	1.351	19	82	HS-VA	fused	PVG
EP5_26	0.917	0.692	1.803	1.251	22	>90	HS-VA	blocky	DCR
EP5_27	0.973	0.740	1.665	1.283	26	>90	HS-VA	blocky	DCR
EP5_28	1.066	0.642	2.190	1.504	55	59	LS-VA	fused	MVG

SAMPLE	Rect.	Compact.	Elong.	Circ.	%ves.	%xls	Particle outline	ext. morpho.	Ground. Texture
EP4_2	1.009	0.699	1.980	1.376	41	67	HS-VA	spongy	MVG
EP4_3	0.984	0.667	1.808	1.360	29	>90	HS-VA	blocky	DCR
EP4_4	1.117	0.652	2.254	1.561	45	64	LS-VA	fused	MVG
EP4_5	0.973	0.682	2.227	1.337	29	61	HS-VA	fused	PVG
EP4_10	1.017	0.646	2.076	1.433	48	71	HS-VA	fused	MVG
EP4_11	0.938	0.647	1.843	1.321	55	83	HS-VA	spongy	MVG
EP4_12	0.892	0.682	1.754	1.220	31	47	HS-SR	blocky	PVG
EP4_13	1.001	0.670	2.071	1.382	52	57	HS-VA	fused	MVG
EP4_14	0.966	0.710	1.956	1.310	28	>90	HS-VA	blocky	DCR
EP4_16	0.873	0.738	1.787	1.149	19	54	HS-SR	blocky	PVG
EP4_17	1.104	0.606	2.127	1.607	44	69	LS-VA	fused	MVG
EP4_18	0.922	0.707	1.840	1.238	40	68	HS-SR	blocky	MVG
EP4_19	0.980	0.557	2.593	1.497	n.d.	n.d.	LS-VA	fused	n.d
EP4_20	0.987	0.711	1.711	1.321	19	>90	HS-VA	blocky	DCR
EP4_21	0.896	0.673	1.745	1.234	36	>90	HS-SR	fused	DCR
EP4_22	0.919	0.750	1.561	1.198	35	>90	HS-SR	blocky	DCR
EP4_23	1.171	0.723	2.119	1.557	31	65	LS-VA	blocky	PVG
EP4_24	0.976	0.545	3.281	1.525	27	56	LS-VA	fused	PVG
EP4_25	0.907	0.666	2.443	1.285	23	>90	HS-VA	blocky	DCR
EP4_26	0.919	0.582	2.620	1.363	37	84	LS-VA	blocky	MVG
EP4_27	1.108	0.612	2.346	1.604	23	63	LS-VA	fused	PVG
EP4_28	1.035	0.634	2.422	1.469	41	70	HS-VA	fused	MVG
EP4_29	1.172	0.717	2.059	1.569	n.d.	n.d.	LS-VA	fused	n.d
EP4_30	0.947	0.612	2.260	1.383	49	59	HS-VA	fused	MVG
EP4_31	0.988	0.629	2.396	1.421	30	45	HS-VA	blocky	PVG
EP4_32	0.948	0.605	2.023	1.382	48	68	LS-VA	fused	MVG
EP4_33	1.085	0.593	2.041	1.597	58	90	LS-VA	spongy	DCR

SAMPLE	Rect.	Compact.	Elong.	Circ.	%ves.	%xls	Particle outline	ext. morpho.	Ground. Texture
EP6_1	0.945	0.640	1.966	1.334	18	57	HS-VA	fused	PVG
EP6_2	0.895	0.651	1.717	1.253	18	75	HS-SR	fused	PVG
EP6_3	0.939	0.705	2.587	1.308	30	63	HS-VA	fused	PVG
EP6_5	0.966	0.610	1.944	1.397	27	83	HS-VA	blocky	PVG
EP6_6	0.904	0.698	1.640	1.222	35	58	HS-SR	blocky	PVG
EP6_7	0.966	0.572	2.762	1.461	13	79	LS-VA	fused	PVG
EP6_8	0.991	0.629	2.987	1.477	41	78	LS-VA	blocky	MVG
EP6_9	0.928	0.706	2.041	1.267	34	82	HS-SR	spongy	PVG
EP6_10	0.962	0.703	1.980	1.296	21	57	HS-VA	blocky	PVG
EP6_11	0.993	0.713	2.012	1.329	47	63	HS-VA	fused	MVG
EP6_12	1.032	0.712	1.795	1.382	49	66	HS-SR	fused	MVG
EP6_13	0.961	0.710	1.791	1.288	39	78	HS-VA	blocky	MVG
EP6_14	0.997	0.653	2.329	1.412	29	74	HS-VA	fused	PVG
EP6_15	0.899	0.694	1.852	1.222	48	79	HS-SR	blocky	MVG
EP6_16	0.980	0.649	2.126	1.378	41	66	HS-VA	blocky	MVG
EP6_17	0.959	0.656	2.222	1.356	40	78	HS-VA	fused	MVG
EP6_18	0.990	0.622	1.847	1.417	27	82	HS-VA	fused	PVG
EP6_19	1.019	0.686	2.027	1.398	30	68	HS-VA	fused	PVG
EP6_20	0.929	0.687	1.646	1.266	21	62	HS-SR	blocky	PVG
EP6_21	0.987	0.791	1.883	1.270	19	>90	HS-SR	blocky	DCR
EP6_22	1.129	0.616	2.350	1.625	45	68	LS-VA	fused	MVG
EP6_23	0.905	0.747	1.640	1.183	32	75	HS-SR	blocky	MVG
EP6_24	1.026	0.541	2.193	1.574	n.d.	n.d.	LS-VA	spongy	n.d
EP6_25	0.970	0.701	1.770	1.310	34	90	HS-VA	spongy	PVG
EP6_26	1.005	0.674	1.861	1.387	25	81	HS-VA	blocky	PVG
EP6_27	1.032	0.563	2.254	1.553	41	72	LS-VA	spongy	MVG
EP6_28	0.978	0.559	2.378	1.484	40	59	LS-VA	fused	MVG
EP6_29	0.963	0.534	2.613	1.491	26	71	LS-VA	fused	PVG
EP6_30	1.035	0.762	1.605	1.338	56	54	HS-SR	fused	MVG

	MVG		PVG		DCR	
wt%	mean (n=13)	σ	mean (n=6)	σ	mean (n=13)	σ
SiO_2	47.63	0.32	47.95	0.34	47.72	0.94
TiO_2	0.95	0.07	0.96	0.05	0.94	0.19
Al_2O_3	20.10	0.26	20.21	0.13	20.31	0.58
FeO	8.44	0.28	8.34	0.15	9.05	1.24
MnO	0.24	0.06	0.28	0.08	0.32	0.07
MgO	1.35	0.09	1.24	0.16	1.02	0.28
CaO	7.92	0.35	7.75	0.46	6.26	1.44
Na_2O	6.59	0.29	6.98	0.51	7.93	1.30
K_2O	5.47	0.44	4.99	0.47	5.14	0.68
P_2O_5	0.14	0.05	0.11	0.06	0.04	0.08
Cl	1.16	0.04	1.19	0.06	1.27	0.12
sum	100		100		100	